J. Appl. Comput. Mech., 12(1) (2026) 255-270
DOI: 10.22055/jacm.2025.48166.5025

ISSN: 2383-4536
jacm.scu.ac.ir

Shahid Chamran University of Ahvaz

Journal of Applied and Computational Mechanics

Research Paper

Effect of a Periodic Magnetic Field on Natural Convection in a Hexagonal Cavity Containing a Nanohybrid Fluid

Bouchmel Mliki[1,2], Mokhtar Ferhi[3], Mohamed Ammar Abbassi[1]

[1] Research Lab, Technology Energy and Innovative Materials, Faculty of Sciences, University of Gafsa, Tunisia
[2] CORIA, Normandie Université, INSA de Rouen, Technopôle du Madrillet, BP 8, Saint-Etienne-du-Rouvray 76801, France
[3] Research Lab, Modeling, Optimization and Augmented Engineering, ISLAIB, University of Jendouba, Béja 9000, Tunisia

Received January 19 2025; Revised March 30 2025; Accepted for publication May 27 2025.
Corresponding author: B. Mliki (bouchmelmliki1986@gmail.com)

Abstract. This article examines natural, laminar, and unsteady convective heat transfer in a hexagonal cavity filled with an Al_2O_3-Ag-water nanohybrid under the influence of a periodic magnetic field. The inclined walls of the cavity are maintained at a constant low temperature, the bottom wall is uniformly heated, and the top wall is considered adiabatic. The dimensionless equations governing the system were solved using the lattice Boltzmann method. The results illustrate the variation of the average Nusselt number (Nu_m), streamlines, and isotherms. The study analyzes the effects of key parameters, including the Rayleigh number (Ra), Hartmann number (Ha), magnetic field period (λ), inclination angle of the cavity (γ) and nanoparticle volume fraction (ϕ), on the flow and heat transfer characteristics. The numerical results show a significant increase in the average Nusselt number with the increase in nanoparticle volume fraction and Rayleigh number. In contrast, the Hartmann number and the cavity inclination angle have opposing effects. Moreover, the numerical results have been proven that the period of the magnetic field significantly affects the heat transfer efficiency in the studied system. Finally, at high Rayleigh numbers (Ra = 10^6), the tilt angle γ significantly affects heat transfer, resulting in a reduction of more than 32% as γ varies from 0 to $3\pi/4$.

Keywords: Heat transfer, Periodic magnetic field, Lattice Boltzmann Method, Hexagonal cavity, Nanohybrid fluid.

1. Introduction

The fluid flow over a hexagonal cavity and its hydrothermal effects plays a crucial role in various technical and engineering applications, such as solar collectors, nuclear power plants, heat exchangers, and microfluidic heat sinks [1-7]. Convection is the primary mode of heat transfer in these systems, making temperature control essential for their operation. To achieve high efficiency while maintaining a compact size, several strategies can be employed. These include optimizing heat exchange surfaces or using fluids with high thermal conductivity instead of conventional ones like water or oil. To develop an efficient heat transfer fluid, we combined nanoscale materials with a base fluid, resulting in Nanohybrids.

For this reason, extensive research has been dedicated to studying heat transfer phenomena in this type of geometry [8-12]. Afraz et al. [8] examined the characteristics of entropy generation and heat fluxes in a magnetized hybrid nanofluid confined within a closed hexagonal cavity containing a cylinder. Their results indicate that an increase in the magnetic field effect reduces heat transfer. Furthermore, a higher Hartmann number leads to an increase in entropy generation. Manoj et al. [9] examined the same phenomenon, considering the effects of cold diamond-shaped obstacles and a periodic magnetic field. The upper inclined walls of the cavity are uniformly heated, while the lower inclined walls serve as heaters. The straight upper and lower walls of the cavity are adiabatic. The numerical solution was obtained using the finite element method. They found that the average Nusselt number increases by 76,16% as the Rayleigh number rises from 10^5 to 10^6 when varying lengths of the hot surface. In another study, Mehryan et al. [10] conducted a statistical and numerical investigation to analyze the optimization and sensitivity of unsteady laminar natural convection heat transfer of Fe_3O_4-water nanofluid in a hexagonal cavity, considering the effects of an inclined magnetic field. The numerical results reveal a significant increase in the average Nusselt number with an increase in the nanoparticle volume fraction, the magnetic field inclination angle, and the Rayleigh number. Conversely, the Hartmann number and nanoparticle diameter exhibit opposite effects. Saleh et al. [11] analyzed the thermal behavior of a hexagonal cavity filled with a nanofluid using the finite element method. Their results show that the application of the magnetic field reduces the intensity of fluid movement, leading to a decrease in flow velocity. Khan et al. [12] also applied the same method to analyze the heat transfer of fluid in a hexagonal cavity with a square obstacle. They noted that the system's kinetic energy increases with higher values of Gr, while the Reynolds number has an opposite effect on this energy.

Published online: May 31 2025

Other recent studies have been conducted on confined cavities filled with hybrid nanofluid, exploring various geometries. They have shown that adding different nanohybrid particles can alter the thermal and mechanical properties of the fluid, thereby influencing the overall heat transfer efficiency [13-15]. Arifin et al. [16] analyzed the natural convection of Casson hybrid nanofluid in a trapezoidal cavity with a partially heated wall. They found that the flow circulation of the Casson hybrid nanofluid inside the trapezoidal cavity increases with higher values of Ra and ϕ. In another study published by Mliki et al. [17], the authors conducted an investigation similar to that carried out by Islam et al. [15]. Their parametric study revealed that the Rayleigh number, Hartmann number, and nanoparticle volume fraction significantly affect thermal transfer in the studied geometry. Using the Lattice Boltzmann method, Khan et al. [18] investigated natural convection heat transfer and entropy generation in a cavity filled with hybrid nanofluid. They observed that the mean Nusselt number increases with the increase in Rayleigh number, while it decreases as the aspect ratio increases. Additionally, Mliki et al. [19] used the same method to examine the impact of a magnetic hybrid nanofluid (Al_2O_3-Cu/H_2O) on natural convection and entropy generation in a square enclosure with a hot obstacle. They observed that heat transfer increases with the Rayleigh number, while it decreases as the Hartmann number increases. Haque et al. [20] conducted a numerical study on a rectotrapezoidal enclosure filled with hybrid nanofluid. They concluded that the hybrid nanoparticle volume fraction and the magnetic field period enhanced the heat transfer rate and efficiency index due to the increased pumping force. In another study, Mliki et al. [21] investigated natural convection under the influence of a uniform magnetic field in a linearly heated square cavity. They found that heat transfer decreased with an increase in the Hartmann number. Miri et al. [22, 23] conducted numerical studies on forced convection, with results showing that both heat transfer and the maximum circulation strength decreased as the intensity of the external magnetic field (Ha) increased. Recently, Das et al. [24] used the commercial finite element solver "COMSOL Multiphysics 6.0" to investigate MHD mixed convection in a semicircular cavity filled with hybrid nanofluids. They observed that heat transfer increases with the Richardson number (Ri), indicating a significant relationship between fluid motion and thermal transfer. Conversely, they also noted that heat transfer decreases as the Hartmann number (Ha) increases. This is due to the stabilizing effect of the magnetic field on the fluid, which inhibits convective movements. In another study, Abood et al. [25] examined the mixed convection phenomenon of a hybrid nanofluid flowing through a horizontally oriented channel. They observed that the average Nusselt number increases with higher Reynolds numbers, angular rotation speeds, cylinder positions, and Richardson numbers. Mliki et al. [26] examined the impact of a horizontal periodic magnetic field in a double lid U-shaped enclosure. By comparing scenarios that account for and neglect the effect of Brownian motion, they found that Brownian motion contributes to the improvement of heat transfer under all defined conditions. As part of the study on the impact of surface roughness on heat transfer, a relevant study was conducted by Omle et al. [27], which explored the effect of triangular roughness inspired by the design of silver ants on the interaction between free convection and surface radiation in a square cavity. The results show that surface roughness significantly affects the thermodynamic and hydrodynamic behavior of the fluid inside the cavity, leading to a reduction in heat transfer of up to 49.9%, particularly when the angles of the triangular roughness are less than 85°.

On the other hand, Ighris et al. [28-29] have explored the application of the lattice Boltzmann method to model natural convection of hybrid nanofluids, highlighting the advantages of this approach in terms of numerical stability and accuracy. In another work Hadoui et al. [30] studied natural double diffusive convection in a square cavity using an Al_2O_3-water based nanofluid. The study was conducted numerically with the lattice Boltzmann method, utilizing the BGK operator. The results indicated that the heat transfer rate increased, while the mass transfer rate decreased with the nanoparticle volume fraction.

A review of the existing literature reveals a significant gap in the study of free convection flow within a nanohybrid-saturated hexagonal cavity under the influence of a periodic magnetic field. This study aims to address this gap by proposing a numerical analysis based on the Boltzmann method to elucidate the thermal and dynamic mechanisms governing these complex flows. The results will not only enhance the understanding of the interactions between hybrid nanofluids and periodic magnetic fields but also provide a solid foundation for optimizing cooling systems and energy conversion in magnetic environments.

The practical application of periodic external magnetic fields in nanohybrids focuses on optimizing heat transfer systems. These systems are utilized in a wide range of applications, such as thermal management of electronic devices, engine and turbine cooling, and the design of heating and cooling systems.

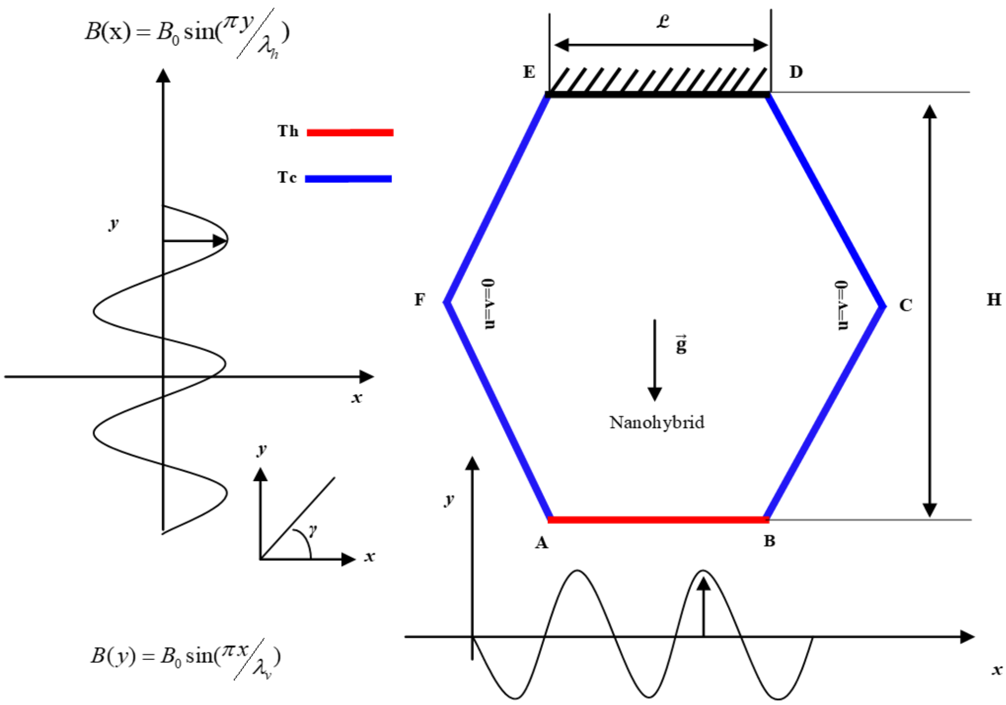

Fig. 1. Geometry of the problem.

Table 1. Thermophysical properties of fluid and nanoparticles [31-33].

Physical properties	Fluid phase (H_2O)	Nanoparticle (Al_2O_3)	Nanoparticle (Ag)
C_p (J / kg.K)	4179	765	235
ρ (kg / m^3)	997.1	3970	10500
k (W / m.K)	0.631	40	429
$\beta \times 10^{-5}$ (1 / K)	21	0.85	1.9
σ $(\Omega / \mathrm{m})^{-1}$	0.05	10^{-10}	6.3×10^{-7}

Velocity boundary conditions:

- **No-slip condition:** u=v=0 (for all walls).

Thermal boundary conditions:

- **For adiabatic walls:** ∂T/∂n=0
- **For isothermal walls:** $T=T_{wall}$

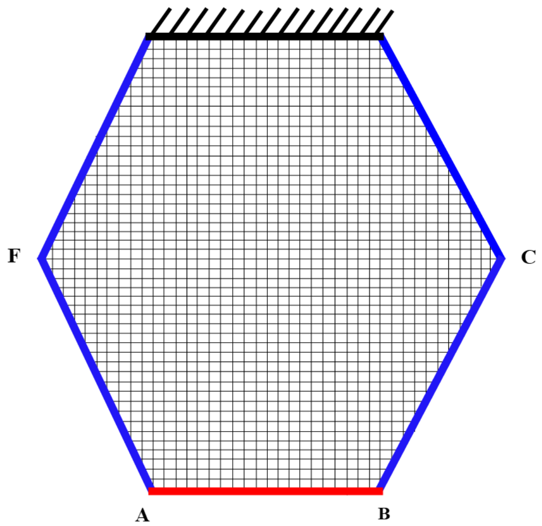

Fig. 2. Boundary conditions and mesh of the studied model.

2. Problem Description

The study focuses on the two-dimensional characterization of heat transfer through free convection inside a hexagonal cavity filled with Al_2O_3-Ag-water nanohybrid (Fig. 1). The inclined walls of the cavity (BC, CD, EF, and FA) are kept at a constant low temperature, the bottom wall (AB) is heated uniformly, and the top wall (DE) is assumed to be adiabatic with a dimension of $L = 0.5L$. Two periodic magnetic fields, one horizontal with a period λ_h and the other vertical with a period λ_v, are respectively applied to the cavity. Gravity acted in the opposite direction of the y-axis. In our study, we use a uniform mesh, as shown in Fig. 2. Table 1 shows the thermo-physical properties of base fluid, Al_2O_3 and Ag nanoparticles.

3. Mathematical Formulation

To investigate natural convection flow, several assumptions are made to simplify the analysis. It is assumed that the fluid flow is incompressible, laminar, and two-dimensional. Additionally, the effects of viscous dissipation, radiation, Joule heating, and induced electric currents are considered negligible in this study [34, 35]. Using the Boussinesq approximation, the governing equations for this investigation are as follows:

$$\frac{\partial u}{\partial x} + \frac{\partial v}{\partial y} = 0 \tag{1}$$

$$\rho_{na\_hy}\left(u\frac{\partial u}{\partial x} + v\frac{\partial u}{\partial y}\right) = -\frac{\partial p}{\partial x} + \mu_{na\_hy}\left(\frac{\partial^2 u}{\partial x^2} + \frac{\partial^2 u}{\partial y^2}\right) + F_x + f_{Lx} \tag{2}$$

$$\rho_{na\_hy}\left(u\frac{\partial v}{\partial x} + v\frac{\partial v}{\partial y}\right) = -\frac{\partial p}{\partial y} + \mu_{na\_hy}\left(\frac{\partial^2 v}{\partial x^2} + \frac{\partial^2 v}{\partial y^2}\right) + F_y + f_{Ly} \tag{3}$$

$$u\frac{\partial T}{\partial x} + v\frac{\partial T}{\partial y} = \alpha_{na\_hy}\left(\frac{\partial^2 T}{\partial x^2} + \frac{\partial^2 T}{\partial y^2}\right) \tag{4}$$

For this problem, the fluid flow is subjected to gravitational force as:

$$F_x = (\rho\beta)_{na\_hy}\, g_y (T - T_c)\sin\gamma \tag{5}$$

$$F_y = (\rho\beta)_{na\_hy}\, g_y (T - T_c)\cos\gamma \tag{6}$$

In addition to the gravitational force, the flow of the nanohybrid is subjected to the volumetric Laplace force as:

$$\text{when the magnetic field is applied vertically: } f_{Lx} = -uB_0^2.\sigma_{na\_hy}\sin^2\left(\frac{\pi x}{\lambda}\right) \tag{7}$$

$$\text{when the magnetic field is applied horizontally: } f_{Ly} = -\upsilon B_0^2.\sigma_{na\_hy}\sin^2\left(\frac{\pi y}{\lambda}\right) \tag{8}$$

To calculate this volumetric Laplace force, it is more appropriate to use the dimensionless Hartmann number, defined by:

$$Ha = HB\sqrt{\sigma_{na\_hy}/\mu_{na\_hy}} \tag{9}$$

This number is used in fluid dynamics, particularly in the study of conducting fluids in the presence of a magnetic field. It characterizes the influence of magnetic forces in relation to viscous forces within a fluid, where σ_{na_hy} is the electrical conductivity, B is the magnetic field intensity, H denotes the characteristic length of the cavity, and μ_{na_hy} is dynamic viscosity of the hybrid nanofluid. The dimensional boundary conditions are determined as follows:

$$\text{Hot wall } AB\text{: } u = \upsilon = 0,\ T = T_h \tag{10}$$

$$\text{Cold walls } BC, CD, EF, FA\text{: } u = \upsilon = 0,\ T = T_c \tag{11}$$

$$\text{Adiabatic wall } DE\text{: } u = \upsilon = 0,\ \partial T/\partial y = 0 \tag{12}$$

Numerical analysis has been conducted using the following dimensionless variables:

$$\begin{gathered} X = \frac{x}{H},\quad Y = \frac{y}{H},\quad U = \frac{uH}{\alpha_{na\_hy}},\quad V = \frac{\upsilon H}{\alpha_{na\_hy}},\quad \theta = \frac{T - T_c}{T_h - T_c},\quad P = \frac{pH^2}{\rho_{na\_hy}\alpha_{na\_hy}^2} \\ Pr = \frac{\nu_{na\_hy}}{\alpha_{na\_hy}},\quad Ra = \frac{g\beta(T - T_c)H^3}{\nu_{na\_hy}\alpha_{na\_hy}},\quad Ha = HB\sqrt{\frac{\sigma_{na\_hy}}{\mu_{na\_hy}}},\quad \lambda = \frac{\lambda_0}{H} \end{gathered} \tag{13}$$

The Rayleigh number (Ra) is a dimensionless parameter that characterizes the balance between buoyancy-driven flow (natural convection) and thermal conduction (diffusion) within a fluid.

Introducing the above dimensionless variables, the non-dimensional forms of the governing equations (1) to (4) are reduced as follows:

$$\frac{\partial U}{\partial X} + \frac{\partial V}{\partial Y} = 0 \tag{14}$$

$$U\frac{\partial U}{\partial X} + V\frac{\partial U}{\partial Y} = -\frac{\partial P}{\partial X} + Pr^*\left(\frac{\partial^2 U}{\partial X^2} + \frac{\partial^2 U}{\partial Y^2}\right) + F_x^* + f_{Lx}^* \tag{15}$$

$$U\frac{\partial V}{\partial X} + V\frac{\partial V}{\partial Y} = -\frac{\partial P}{\partial Y} + Pr^*\left(\frac{\partial^2 V}{\partial X^2} + \frac{\partial^2 V}{\partial Y^2}\right) + F_y^* + f_{Ly}^* \tag{16}$$

$$U\frac{\partial \theta}{\partial X} + V\frac{\partial \theta}{\partial Y} = \left(\frac{\partial^2 \theta}{\partial X^2} + \frac{\partial^2 \theta}{\partial Y^2}\right) \tag{17}$$

where,

$$F_x^* = Ra^* Pr^* \theta \sin\gamma \tag{18}$$

$$F_y^* = Ra^* Pr^* \theta \cos\gamma \tag{19}$$

$$f_{Lx}^* = -Ha^2 Pr^* \sin^2\left(\frac{\pi X}{\lambda_0}\right)U \tag{20}$$

$$f_{Ly}^* = -Ha^2 Pr^* \sin^2\left(\frac{\pi Y}{\lambda_0}\right)V \tag{21}$$

$$Pr^* = \frac{\mu_{nf}}{\mu_f}\frac{C_{p_{nf}}}{C_{p_f}}\frac{k_f}{k_{nf}}Pr,\quad Ra^* = \frac{(\rho\beta)_{nf}}{(\rho\beta)_f}\frac{k_f}{k_{nf}}\frac{(\rho C)_{p_{nf}}}{(\rho C)_{p_f}}\frac{\mu_f}{\mu_{nf}}Ra \tag{22}$$

The non-dimensional boundary conditions are calculated as follows:

$$\text{Hot wall } AB\text{: } U = V = 0,\ \theta = 1 \tag{23}$$

$$\text{Cold walls } BC, CD, EF, FA\text{: } U = V = 0,\ \theta = 0 \tag{24}$$

$$\text{Adiabatic wall } DE\text{: } U = V = 0,\ \partial\theta / \partial Y = 0 \tag{25}$$

Local and average Nusselt numbers along the hot wall (AB) are calculated by:

$$Nu_m = -\frac{k_{nf}}{k_f}\left(\frac{\partial\theta}{\partial Y}\right)\Bigg|_{Y=0} \tag{26}$$

$$\overline{Nu_l} = -\frac{1}{AB}\int_A^B \frac{k_{hnf}}{k_f}\left(\frac{\partial\theta}{\partial Y}dX\right)\Bigg|_{Y=0} \tag{27}$$

The thermophysical properties of hybrid-nanoliquid are defined as follows [17]:

- The effective density is calculated by:

$$\rho_{hnf} = (1-\phi)\rho_f + \phi_{Al_2O_3}\rho_{Al_2O_3} + \phi_{Ag}\rho_{Ag} \tag{28}$$

- The heat capacitance is defined by:

$$\left(\rho Cp_{hnf}\right) = (1-\phi)(\rho Cp)_f + \phi_{Al_2O_3}\left(\rho Cp\right)_{Al_2O_3} + \phi_{Ag}\left(\rho Cp\right)_{Ag} \tag{29}$$

- The thermal expansion coefficient is:

$$(\rho\beta)_{hnf} = (1-\phi)(\rho\beta)_f + \phi_{Al_2O_3}\left(\rho\beta\right)_{Al_2O_3} + \phi_{Ag}\left(\rho\beta\right)_{Ag} \tag{30}$$

where $\phi = \phi_{Al_2O_3} + \phi_{Ag}$, represents the concentration of the nanoparticles that have been added to the base fluid. This concentration is essential, as it significantly affects the thermophysical properties of the fluid.

The dynamic viscosity of the hybrid-nanoliquid is:

$$\mu_{na\_hy} = \frac{\mu_f}{\left(1-\left(\phi_{Al_2O_3} + \phi_{Ag}\right)\right)^{2.5}} \tag{31}$$

The thermal diffusivity is defined by:

$$\alpha_{na\_hy} = \frac{k_{na\_hy}}{(\rho C_p)_{na\_hy}} \tag{32}$$

The definitions for the thermal conductivity and electrical conductivity of the hybrid-nanoliquid are given by [17]:

$$\frac{k_{hnf}}{k_f} = \left[\frac{\left(\dfrac{\phi_{Al_2O_3}k_{Al_2O_3} + \phi_{Ag}k_{Ag}}{\phi} + 2k_f + 2\left(\phi_{Al_2O_3}k_{Al_2O_3} + \phi_{Ag}k_{Ag}\right) - 2\phi k_f\right)}{\left(\dfrac{\phi_{Al_2O_3}k_{Al_2O_3} + \phi_{Ag}k_{Ag}}{\phi} + 2k_f - \left(\phi_{Al_2O_3}k_{Al_2O_3} + \phi_{Ag}k_{Ag}\right) + \phi k_f\right)}\right] \tag{33}$$

$$\frac{\sigma_{hnf}}{\sigma_f} = \left[1 + \frac{3\left(\dfrac{\phi_{Al_2O_3}\sigma_{Al_2O_3} + \phi_{Ag}\sigma_{Ag}}{\sigma_f} - \left(\phi_{Al_2O_3} + \phi_{Ag}\right)\right)}{\left(\dfrac{\phi_{Al_2O_3}\sigma_{Al_2O_3} + \phi_{Ag}\sigma_{Ag}}{\phi\sigma_f} + 2\right) - \left(\dfrac{\phi_{Al_2O_3}\sigma_{Al_2O_3} + \phi_{Ag}\sigma_{Ag}}{\sigma_f} - \left(\phi_{Al_2O_3} + \phi_{Ag}\right)\right)}\right] \tag{34}$$

4. Numerical Method

4.1. Boundary conditions

The given equations have been numerically solved using the lattice Boltzmann method (LBM), as detailed in [36, 37]. This approach was based on Ludwig Boltzmann's kinetic theory of gases. Employing the Bhatnagar-Gross-Krook approximation, the lattice Boltzmann method involves two distribution functions, denoted as g and f, representing the temperature and the flow field, respectively, given by:

$$f_i\left(\mathbf{x} + \mathbf{c}_i\Delta t, t + \Delta t\right) = f_i\left(\mathbf{x}, t\right) - \frac{1}{\tau_\nu}\left(f_i\left(\mathbf{x}, t\right) - f_i^{eq}\left(\mathbf{x}, t\right)\right) + \Delta t\mathbf{c}_i F_i \tag{35}$$

$$g_i\left(\mathbf{x} + \mathbf{c}_i\Delta t, t + \Delta t\right) = g_i\left(\mathbf{x}, t\right) - \frac{1}{\tau_\alpha}\left(g_i\left(\mathbf{x}, t\right) - g_i^{eq}\left(\mathbf{x}, t\right)\right) \tag{36}$$

Here, Δt represents the lattice time, τ_ν and τ_α denote the lattice relaxation times for the flow and temperature fields, respectively.

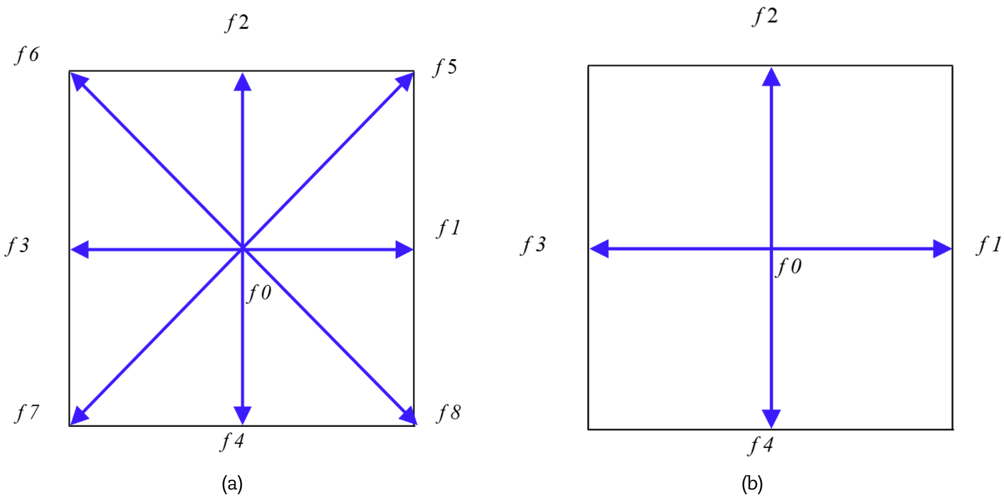

Fig. 3. Direction of streaming velocities, (a) D2Q9, (b) D2Q4.

Two local equilibrium distribution functions for the temperature and flow fields g_i^{eq} and f_i^{eq} are calculated by:

$$f_i^{eq} = \omega_i \rho \left[1 + \frac{3(c_i.u)}{c^2} + \frac{9(c_i.u)^2}{2c^4} - \frac{3u^2}{2c^2} \right] \tag{37}$$

$$g_i^{eq} = \omega_i^{'} T \left[1 + 3\frac{c_i.u}{c^2} \right] \tag{38}$$

The variables u and ρ represent the macroscopic velocity and density, respectively. The lattice speed c is defined as $c = \Delta x/\Delta t$, where Δx is the lattice spacing and Δt is the lattice time step, both of which are set to unity. Furthermore, ω_i denotes the weighting factor for the flow field, while $\omega_i^{'}$ represents the weighting factor for the temperature field. The D2Q9 model is used for the flow field, while the D2Q4 model is applied to the temperature field. Consequently, the weighting factors and discrete particle velocity vectors differ between these two models and are calculated using as follows:

- For D2Q9:

$$\omega_0 = \frac{4}{9},\ \omega_i = \frac{1}{9} \text{ for } i = 1,2,3,4 \text{ and } \omega_i = \frac{1}{36} \text{ for } i = 5,6,7,8 \tag{39}$$

- The discrete velocities for the D2Q9 (Fig. 3(a)) are defined as follows:

$$\mathbf{c}_i = \begin{cases} 0 & i = 0 \\ (\cos[(i-1)\pi/2], \sin[(i-1)\pi/2])c & i = 1,2,3,4 \\ \sqrt{2}\left(\cos[(i-5)\pi/2 + \pi/4], \sin[(i-5)\pi/2 + \pi/4]\right)c & i = 5,6,7,8 \end{cases} \tag{40}$$

- For D2Q4:

$$\text{The weighting factor for temperature in each direction is: } \omega_i^{'} = \frac{1}{4} \tag{41}$$

- The discrete velocities for the D2Q4 (Fig. 3(b)) are defined as follows:

$$\mathbf{c}_i = (\cos[(i-1)\pi/2], \sin[(i-1)\pi/2])c \qquad i = 1,2,3,4 \tag{42}$$

The relationship between the kinematic viscosity ν and thermal diffusivity α with the relaxation time is expressed by:

$$\nu = \left[\tau_\nu - \frac{1}{2}\right] c_s^{\,2} \Delta t, \quad \alpha = \left[\tau_\alpha - \frac{1}{2}\right] c_s^{\,2} \Delta t \tag{43}$$

where c_s is the lattice speed of sound, equal to $c_s = c/\sqrt{3}$. In the simulation of natural convection, the external force term F_i is determined by:

$$F_i = \frac{\omega_i}{c_s^{\,2}} F.c_i \tag{44}$$

with F is the total external body force. The macroscopic quantities ρ, u and T can be calculated by:

$$\rho = \sum_i f_i; \quad \rho u = \sum_i f_i c_i; \quad T = \sum_i g_i \tag{45}$$

4.2. Boundary conditions

The implementation of boundary conditions is crucial for the simulation.

4.2.1. Flow

Bounce-back boundary conditions were applied to all solid walls. This implies that the incoming particle populations at the boundaries are equal to the outgoing populations after the collision:

$$\text{Wall AB: } f_2(i,0)=f_4(i,0) \quad ; \quad f_5(i,0)=f_7(i,0) \quad ; \quad f_6(i,0)=f_6(i,0) \tag{46}$$

$$\text{Wall BC: } f_2(i,j)=f_4(i,j) \quad ; \quad f_6(i,j)=f_8(i,j) \quad ; \quad f_3(i,j)=f_1(i,j) \tag{47}$$

$$\text{Wall CD: } f_3(i,j)=f_1(i,j) \quad ; \quad f_7(i,j)=f_5(i,j) \quad ; \quad f_4(i,j)=f_2(i,j) \tag{48}$$

$$\text{Wall EF: } f_1(i,j)=f_3(i,j) \quad ; \quad f_8(i,j)=f_6(i,j) \quad ; \quad f_4(i,j)=f_2(i,j) \tag{48}$$

$$\text{Wall FA: } f_2(i,j)=f_4(i,j) \quad ; \quad f_5(i,j)=f_7(i,j) \quad ; \quad f_1(i,j)=f_3(i,j) \tag{50}$$

$$\text{Wall AB: } f_7(i,0)=f_5(i,m) \quad ; \quad f_4(i,m)=f_2(i,m) \quad ; \quad f_8(i,m)=f_6(i,m) \tag{51}$$

4.2.2. Temperature

The bounce-back boundary condition is applied to the adiabatic wall. The temperature is specified and known on the isothermal walls. Within the D2Q4 model framework, the unknown internal energy distribution functions are determined as follows:

$$\text{Wall AB: } g_2(i,0)=t_h\left(\omega_2^{'}+\omega_4^{'}\right)-g_4(i,0) \tag{52}$$

$$\text{Wall BC: } g_2(i,j)=t_h\left(\omega_2^{'}+\omega_4^{'}\right)-g_4(i,j); \quad g_3(i,j)=t_h\left(\omega_3^{'}+\omega_1^{'}\right)-g_1(i,j) \tag{53}$$

$$\text{Wall CD: } g_3(i,j)=t_h\left(\omega_3^{'}+\omega_1^{'}\right)-g_1(i,j); \quad g_4(i,j)=t_h\left(\omega_4^{'}+\omega_2^{'}\right)-g_2(i,j) \tag{54}$$

$$\text{Wall EF: } g_1(i,j)=t_h\left(\omega_1^{'}+\omega_3^{'}\right)-g_3(i,j); \quad g_4(i,j)=t_h\left(\omega_4^{'}+\omega_2^{'}\right)-g_2(i,j) \tag{55}$$

$$\text{Wall FA: } g_2(i,j)=t_h\left(\omega_2^{'}+\omega_4^{'}\right)-g_4(i,j); \quad g_1(i,j)=t_h\left(\omega_1^{'}+\omega_3^{'}\right)-g_3(i,j) \tag{56}$$

$$\text{Wall AB: } g_4\left(i,m\right)=g_4\left(i,m-1\right) \tag{57}$$

5. Grid Independent Test and Numerical Verification

As part of the grid sensitivity analysis, Table 2 presents the results obtained using four different mesh sizes for the simulations. These cases were used to assess the impact of mesh size on the accuracy of the numerical results. By comparing the results from meshes of different resolutions, we observed that the difference between the 100 × 100 and 120 × 120 meshes was negligible. This minor variation suggests that increasing the mesh resolution beyond 100 × 100 does not lead to a significant improvement in accuracy, but it does increase computational complexity and the calculation time. Therefore, to optimize the efficiency of the simulations without compromising accuracy, the 100 × 100 mesh size was chosen for the final analysis.

To validate our results, we compared the isotherms obtained for Pr = 6.8 and Ra = 10^5 with those reported by Asha et al. [38] (Fig. 4). Additionally, the average Nusselt number along the heated wall was compared to the numerical results of Ghasemi et al. [39] on magnetic nanofluid convection in a square cavity (Table 3). These comparisons confirm the accuracy and reliability of the developed code for studying MHD natural convection of a Nanohybrid in the examined cavity, especially under the influence of an external magnetic field.

Table 2. Grid independence test for $\overline{Nu}_m$ at ϕ = 4×10^{-2}, Ha = 0, γ = 0.

	Average Nusselt number		
Lattice size	Ra = 10^4	Ra = 10^5	Ra = 10^6
50 × 50	4,0612	4,5411	6,5451
75 × 75	4, 7438 (16, 8%)	5, 8113 (27, 97%)	8, 5157 (30,094%)
100 × 100	4, 9315 (3, 95%)	6, 0459 (4, 036%)	9, 6301 (13,123%)
120 × 120	4, 9708 (0,796%)	6, 1198 (1, 224%)	9, 8345 (2,118%)

Table 3. Validation of the average Nusselt number on the hot wall of the cavity for Ra = 10^5 and ϕ = 0,04

	Ghasemi et al. [39]	Present simulation	Error
Ha = 0	4,896	4,821	1,5%
Ha = 15	4,211	4,138	1,7%
Ha = 30	3,124	3,194	2,1%
Ha = 45	2,317	2,383	2,7%
Ha = 60	2,415	2,467	2,1%

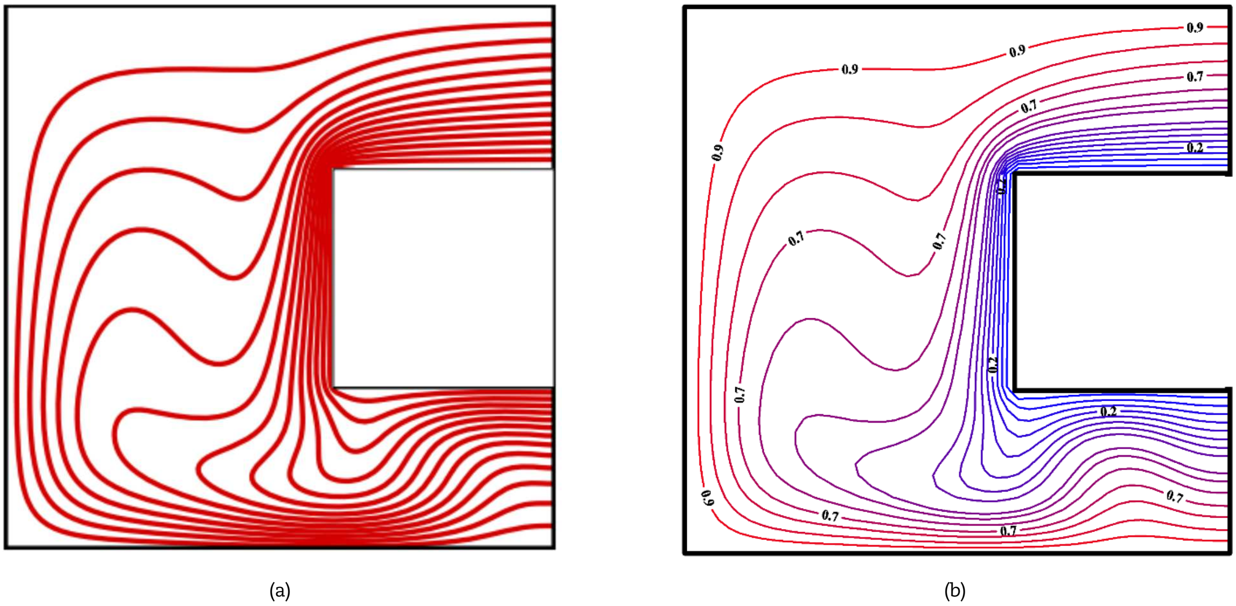

Fig. 4. Comparison of isotherms for the C-shaped cavity for Pr = 6.2, Ha = 0, Ra = 10^5, AR = 0.4, (a) results by Asha et al. [38], (b) Present MHD-LBM.

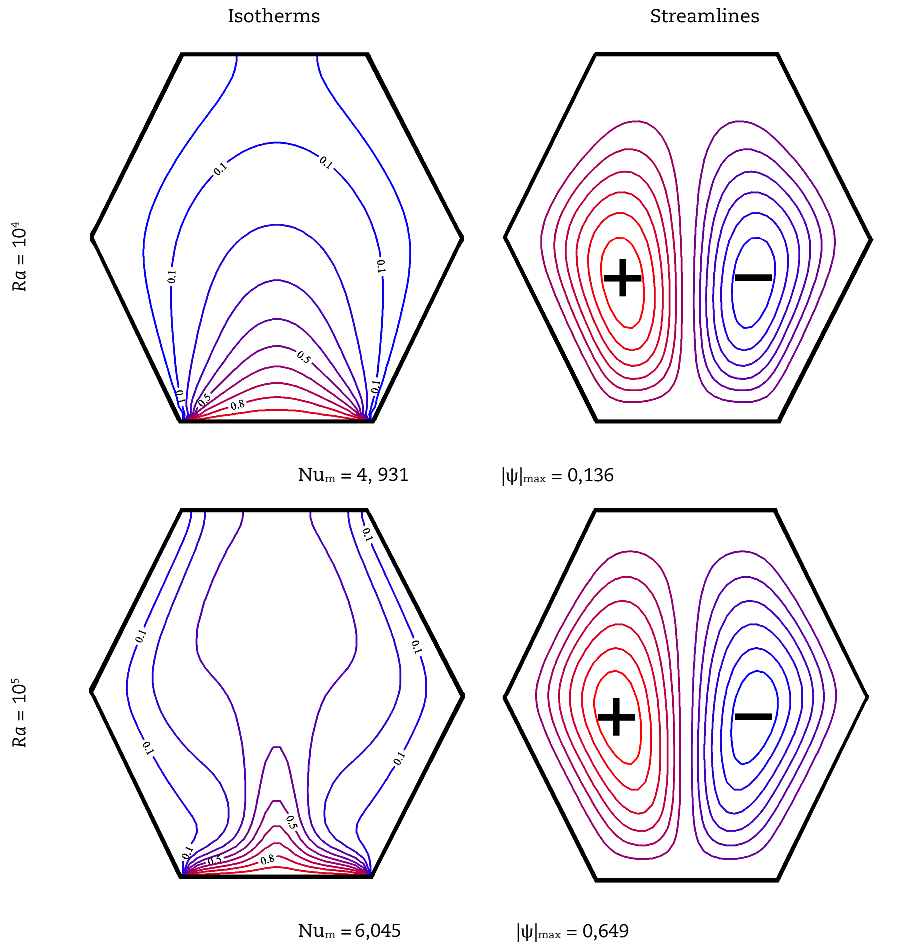

Fig. 5. Effect of the Rayleigh numbers (Ra = 10^4 and 10^5) on the isotherms (left) and streamlines (right) for Ha = 0, γ = 0 and ϕ = 0,04.

6. Results and Discussion

This article focuses on the numerical study of natural convection in a hexagonal cavity containing a nanohybrid fluid. The goal is to investigate the influence of control parameters such as Rayleigh number ($10^3 \le Ra \le 10^6$), nanoparticles volume fraction of ($0 \le \phi \le 0{,}04$), periodic magnetic field ($0{,}25 \le \lambda \le 1$), Hartmann number ($0 \le Ha \le 80$) and inclination angle of the cavity ($0 \le \gamma \le 3\pi/4$) on the enhancement of heat transfer and the control of fluid flow.

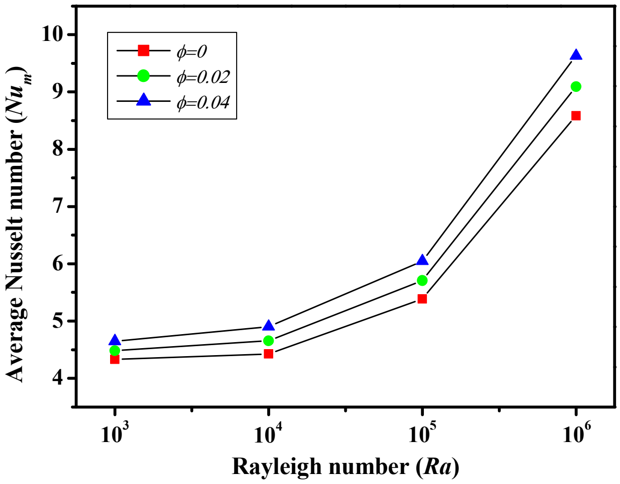

Fig. 6. Average Nusselt number on the hot wall for different Ra at $Ha = 0$ and $\gamma = 0$.

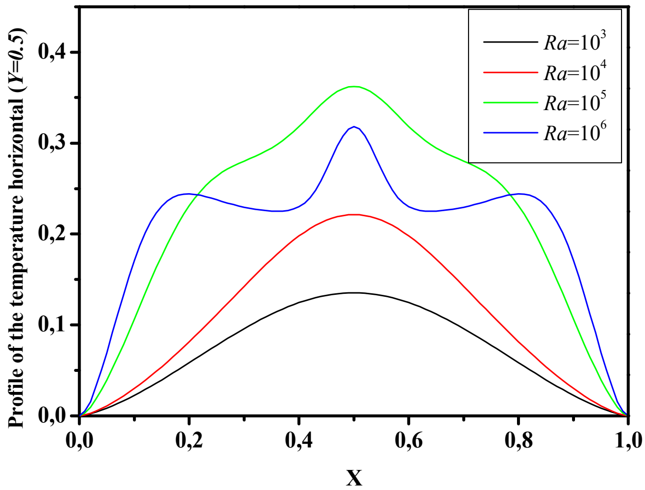

Fig. 7. Profile of the dimensionless temperature in the middle of the cavity ($Y = 0,5$) for different Ra at $Ha = 0$, $\gamma = 0$ and $\phi = 0,04$.

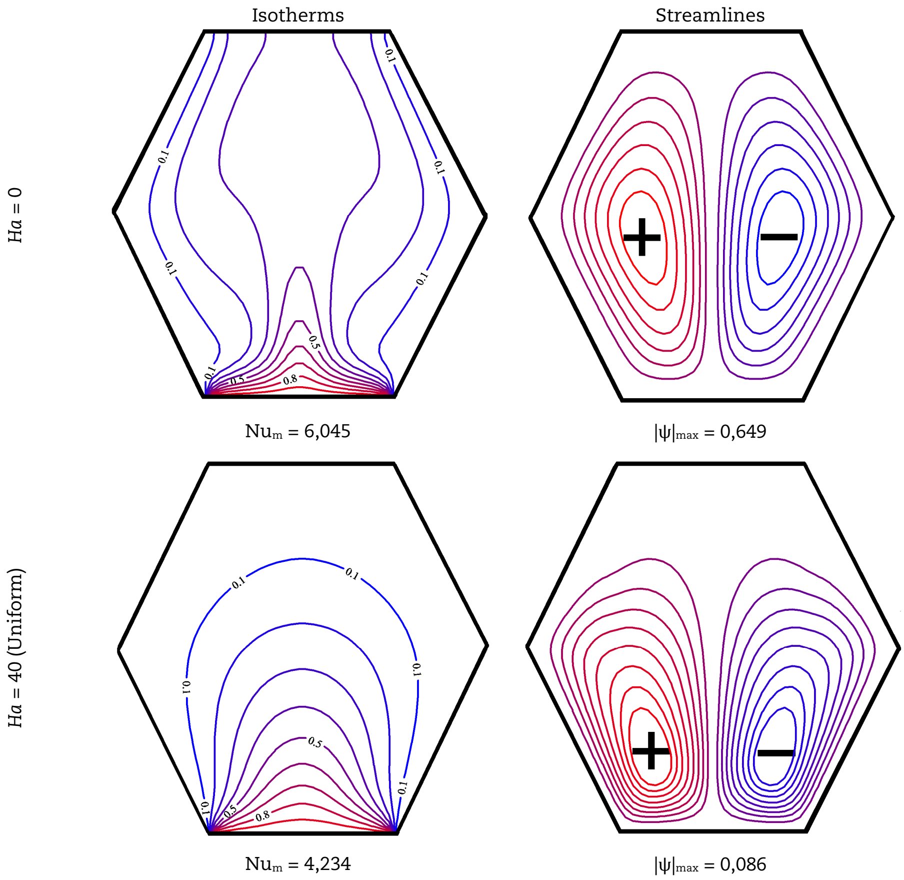

Fig. 8. Effect of the Hartmann number ($Ha = 0$ and 40) (uniform), on the Isotherms (left) and streamlines (right) for $Ra = 10^5$, $\gamma = 0$ and $\phi = 0,04$.

6.1. Effects of Rayleigh number

The vertical mid-plane Y = 0,5 represents a plane of symmetry for the transfer phenomena under study, as shown in Fig. 5. This symmetry leads to a specific flow pattern within the cavity, characterized by the presence of two main recirculation cells. These cells rotate in opposite directions and are symmetric relative to this plane. At a Rayleigh number $Ra = 10^4$, the isotherms are nearly parallel to the isothermal walls and perpendicular to the adiabatic walls. This suggests that the convective forces are too weak to induce significant fluid motion. Consequently, heat transfer within the cavity is predominantly governed by conduction. For $Ra = 10^5$, the effect of the Rayleigh number on the streamlines and isotherms becomes significantly more pronounced compared to $Ra = 10^4$, with noticeable differences between the two cases. The increase in the Rayleigh number intensifies the convective flux, leading to the visible formation of a thermal boundary layer along the walls, particularly near the corners of the heating device [AB]. As a result, convection becomes more dynamic, and heat transfer occurs through both conduction and convection, enabling the fluid to transport thermal energy more efficiently.

The heat transfer rate is evaluated by calculating the average Nusselt number on the wall [AB] for different Rayleigh numbers and nanoparticle volume fractions with Ha = 0 (Fig. 6). The results show that heat transfer increases significantly with higher Rayleigh numbers, particularly for $Ra = 10^6$. Additionally, the presence of nanoparticles improves heat transfer due to the altered thermophysical properties of the nanofluid, especially its thermal conductivity, which is higher than that of the base fluid.

Figure 7 shows the temperature profile at the mid-position Y = 0,5 of the cavity, as a function of the Rayleigh number (Ra). It highlights the evolution of the thermal distribution within the cavity in response to the increase in Ra. It can be observed that increasing this parameter leads to more pronounced heating of the fluid in the upper part of the cavity. However, the fluid temperature in the upper part is lower when $Ra = 10^6$ compared to $Ra = 10^5$. This difference can be attributed to the evolution of the convective flow structure within the cavity: at higher Ra values, the fluid moves faster, generating more complex convection zones and a less uniform temperature distribution, particularly near the upper wall.

6.2. Effects of Hartmann number

The analysis of the streamlines for $Ra = 10^5$, shown in Fig. 8, indicates that an increase in the Hartmann number significantly alters the flow structure within the cavity. Specifically, the two recirculation cells move toward the lower part of the cavity, while a dead zone forms in the upper region, near the DE wall. This dead zone is characterized by low convective activity, indicating a disruption in the natural convection process. This phenomenon can be explained by the fact that the magnetic force is directly proportional to the fluid velocity, which is influenced by the Rayleigh number, the primary parameter driving the flow. As the Hartmann number increases, the magnetic forces apply greater pressure on the fluid, thereby restricting its movement.

This phenomenon disrupts heat transfer by convection, particularly in areas where natural convection was previously dominant. As a result, heat transfer becomes primarily governed by thermal conduction, which is less efficient than convection when transferring thermal energy. This is clearly confirmed by the evolution of the temperature profile at the mid-position Y = 0,5 for $Ra = 10^5$ (Fig. 9). It can be observed that the thermal distribution is strongly influenced by the increase in the Hartmann number. The temperature variation follows the movement of the recirculation cells.

Figure 10 shows the variation of the average Nusselt number as a function of the Hartmann number. This figure demonstrates that an increase in the Hartmann number leads to a decrease in the average Nusselt number, with a notable reduction when $Ha < 40$. As a result, the presence of the magnetic field impedes heat transfer, especially in the convective flow regime. Beyond $Ha > 40$, the average Nusselt number tends toward an asymptotic value of 3,61, independent of the Hartmann number. This can be explained by the fact that the influence of the magnetic field becomes nearly negligible for low-velocity flows (high Hartmann number).

6.3. Effects of horizontal magnetic field period

Figure 11 presents a detailed analysis of the variations in streamlines and isotherms as a function of the period of the horizontal magnetic, under specific conditions defined by ϕ = 0,04, $Ra = 10^5$, and Ha = 40. The results clearly highlight the significant influence of the magnetic field period on the fluid behavior in the studied system.

This analysis highlights the system's pronounced sensitivity to periodic variations in the magnetic field, confirming that this parameter plays a crucial role in controlling and optimizing thermal and dynamic performance. To make a meaningful comparison, Fig. 5 (second row) is used as a reference, showing the streamlines for a uniform magnetic field. This reference configuration enables the analysis of the differences caused by the application of a periodic magnetic field. At a low value of λ (λ = 0,25), the streamlines near the inclined walls are observed to deviate from their trajectory due to the gradient in the variation of the Lorentz force intensity. While the magnetic forces are not strong enough to completely dominate the fluid flow, they are sufficiently powerful to induce a localized deviation in the streamlines.

Figure 12 offers a detailed analysis of the variations in streamlines and isotherms as a function of the period of the vertical magnetic effect, under specific conditions where ϕ = 0,04, $Ra = 10^5$, and Ha = 40. The results highlight the significant influence of the magnetic field period on the fluid behavior within the analyzed system.

Initially, at a low value of λ (λ = 0,25), the circulation cells within the cavity are dominated by symmetric behavior. In this regime, the trajectories of the internal currents follow well-defined paths, resulting in a regular flow where the effects of thermal convection are relatively uniform and predictable. The thermal and fluid properties of the system remain constant and well-controlled, which can be beneficial for applications that require thermal stability, such as in certain cooling system configurations. However, as the period of the magnetic increases, the stability is disrupted. The effect of this periodic magnetic field introduces an influence that affects the moving fluid particles, altering the symmetry of the initially stable flow.

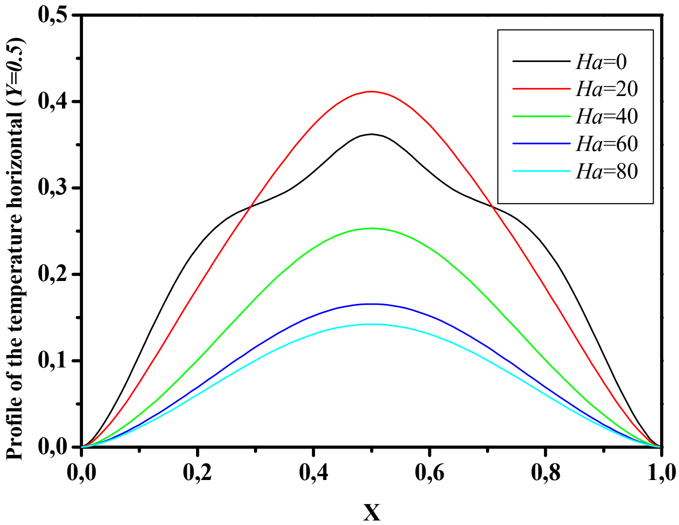

Fig. 9. Profile of the dimensionless temperature in the middle of the cavity (Y = 0,5) for different Ha (uniform) at $Ra = 10^5$, γ = 0 and ϕ = 0,04.

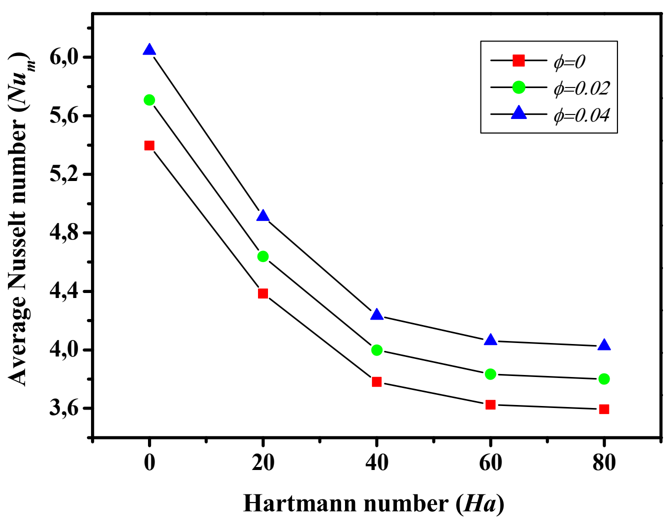

Fig. 10. Average Nusselt number on the hot wall for different Ha (uniform) at for $Ra = 10^5$, γ = 0 and ϕ = 0,04.

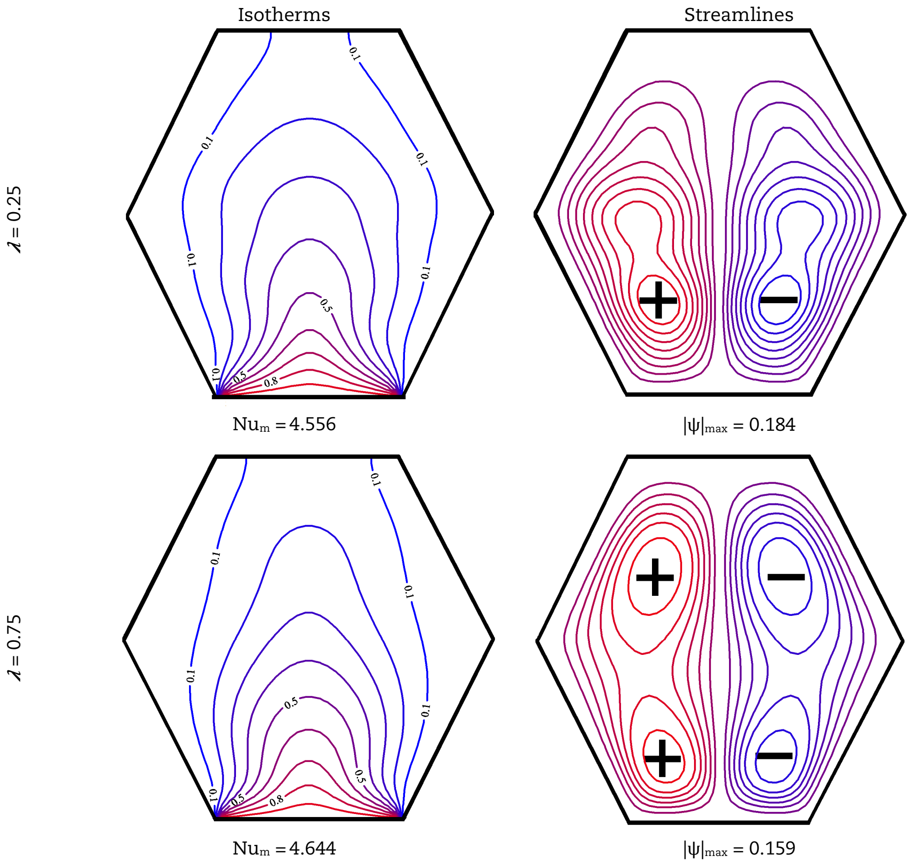

Fig. 11. Isotherms (left) and streamlines (right) for various (horizontal magnetic field) at $\gamma = 0$, $\phi = 0{,}04$, $Ra = 10^5$, and $Ha = 40$.

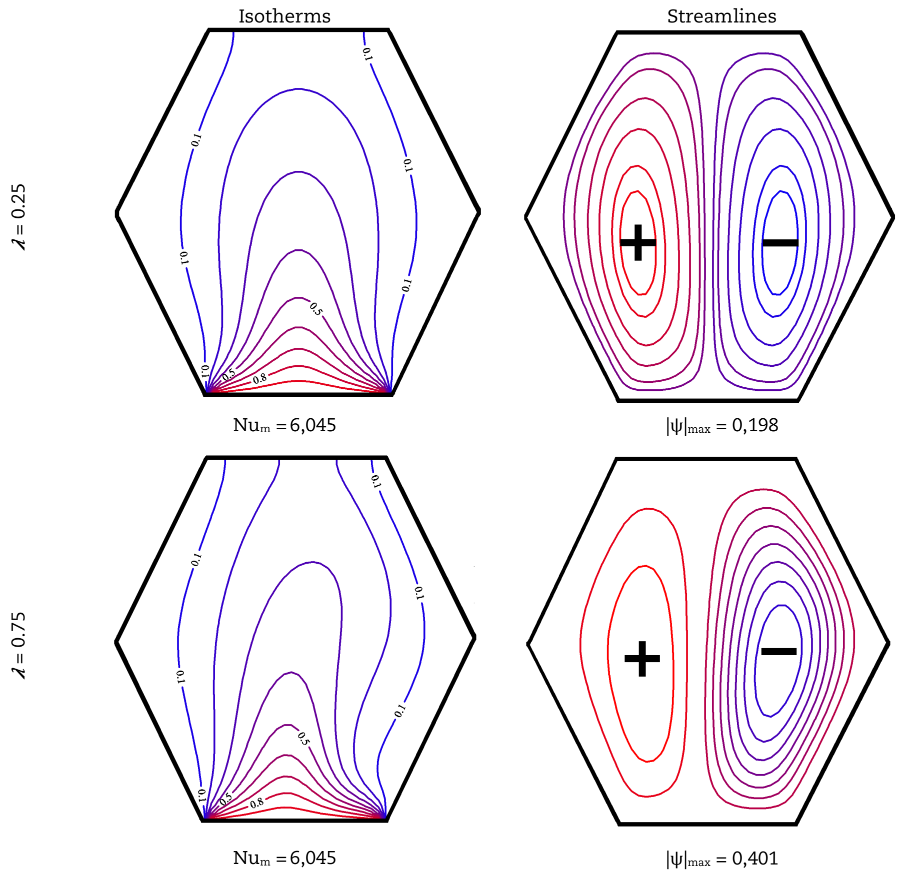

Fig. 12. Isotherms (left) and streamlines (right) for various (vertical magnetic field) at $\gamma = 0$, $\phi = 0{,}04$, $Ra = 10^5$, and $Ha = 40$.

This magnetic disturbance causes a deviation in the trajectories of the internal currents, thereby modifying the behavior of the circulation cells. This deviation phenomenon can lead to several consequences for the system, including a redistribution of heat within the cavity. In other words, the temperature zones are no longer as uniformly distributed, which can affect the system's thermal efficiency.

However, as the period of the magnetic increases, the magnetic field applied to the cavity disrupts this stability. The effect of this periodic magnetic field introduces an influence that affects the moving fluid particles, altering the symmetry of the initially stable flow. This magnetic disturbance causes a deviation in the trajectories of the internal currents, thereby modifying the behavior of the circulation cells. This deviation phenomenon can lead to several consequences for the system, including a redistribution of heat within the cavity. In other words, the temperature zones are no longer as uniformly distributed, which can affect the system's thermal efficiency.

Figure 13 illustrates the evolution of the average Nusselt number on the heated wall for different values of λ. It can be observed that the uniform magnetic effect generates the highest average heat transfer rate. However, as λ increases from 0,25 to 0,50, a progressive decrease in heat transfer is noted. This reduction can be attributed to the modification of the thermal flow configuration within the fluid. Indeed, as λ increases, the distribution of magnetic forces in the fluid becomes less uniform, disrupting the thermal circulation. This redistribution of heat leads to reduced thermal efficiency, as heat is less effectively transported through the fluid.

At λ = 0,50, the Nusselt number reaches its minimum value equal to 3.87, representing the lowest thermal efficiency in the studied range. This phenomenon can be explained by a specific configuration of the thermal flow at this point, where the interaction between the fluid and the magnetic forces is less favorable to heat transfer. This configuration reduces the intensity of thermal convection near the walls, which slows down the heat transfer process. However, as λ increases from 0.50 to 1, an opposite effect begins to manifest. Heat transfer starts to increase again.

This recovery may be due to a gradual adjustment in the distribution of magnetic forces, which promotes better thermal circulation and greater heat transfer efficiency. The magnetic interaction with the fluid becomes more favorable, allowing for better heat distribution and an improvement in the overall thermal efficiency of the system. This behavior highlights the importance of the λ value in optimizing heat transfer, indicating that for certain values, magnetic effects can either reduce or enhance thermal efficiency, depending on the configuration of the magnetic field and the fluid dynamics.

The effects of the vertical magnetic effect period λ on the Nusselt number (Nu_m) are presented in Fig. 14. This study highlights the significant impact of variations in λ on heat transfer efficiency in the analyzed system. Initially, it is observed that as λ increases up to a value of 0,75, heat transfer increases significantly. This increase can be attributed to the beneficial influence of the vertical magnetic field on convective motions. This phenomenon reflects a favorable interaction between the magnetic field and convective processes, resulting in enhanced heat transfer. However, when λ exceeds 0,75 and reaches 1, a change in trend is observed. In this range, heat transfer begins to decrease gradually. This decrease can be explained by the stabilizing effect of the magnetic field as it becomes dominant, limiting the convective circulation of the fluid. Indeed, an excessive magnetic field could partially suppress the natural fluid motions, reducing the thermal transfer efficiency. The maximum value of the Nusselt number (Nu_m), is equal to 4,81 for a period of λ = 0,75. This critical point marks the optimal condition in which heat transfer is most efficient within the studied range. It represents a perfect balance between the amplifying effect of the magnetic field and the convective dynamics of the fluid.

The results presented in this section demonstrate that applying a vertical periodic magnetic field can partially counteract the reduction in heat transfer caused by a uniform magnetic field. Specifically, when λ = 0,75, we observed a 14.52% increase in the heat transfer rate compared to the case with a uniform magnetic field. This improvement suggests that the vertical periodic magnetic field introduces additional dynamics, which help mitigate the negative effects of the uniform field. However, while this improvement is notable, it remains limited. The heat transfer rate achieved with the vertical periodic magnetic field does not exceed the levels observed in the complete absence of a magnetic field. This indicates that, despite its positive impact, the vertical periodic magnetic field does not fully restore heat transfer performance to its optimal level.

6.4 Effects of the inclination angle of the cavity (γ)

We vary the inclination angle γ from 0 to $3\pi/4$ in regular increments of $\pi/4$ while keeping the parameters Ha = 0, Ra = 10^5, and ϕ = 0,04 constant. Figure 15 illustrates the streamlines and isotherms, highlighting the effect of the cavity inclination. It is clear that the isotherms are strongly influenced by the angle γ, leading to changes in the flow direction. For small values of γ (close to 0), the flow is characterized by two contra-rotative cells: the hot fluid rises vertically along the upper wall (DE), while the cold fluid symmetrically descends along the inclined walls. However, as the angle increases, an asymmetry develops in the flow, modifying both the direction and intensity of heat transport.

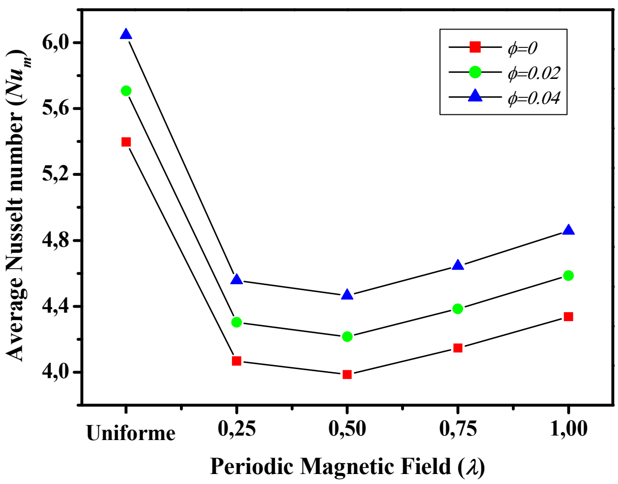

Fig. 13. Average Nusselt number on the hot wall as function of horizontal magnetic field period at γ = 0, Ra = 10^5, and Ha = 40.

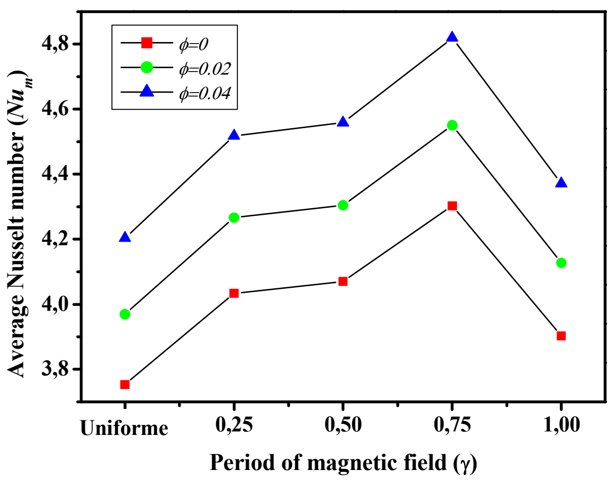

Fig. 14. Average Nusselt number on the hot wall as function of vertical magnetic field period at γ = 0, Ra = 10^5, and Ha = 40.

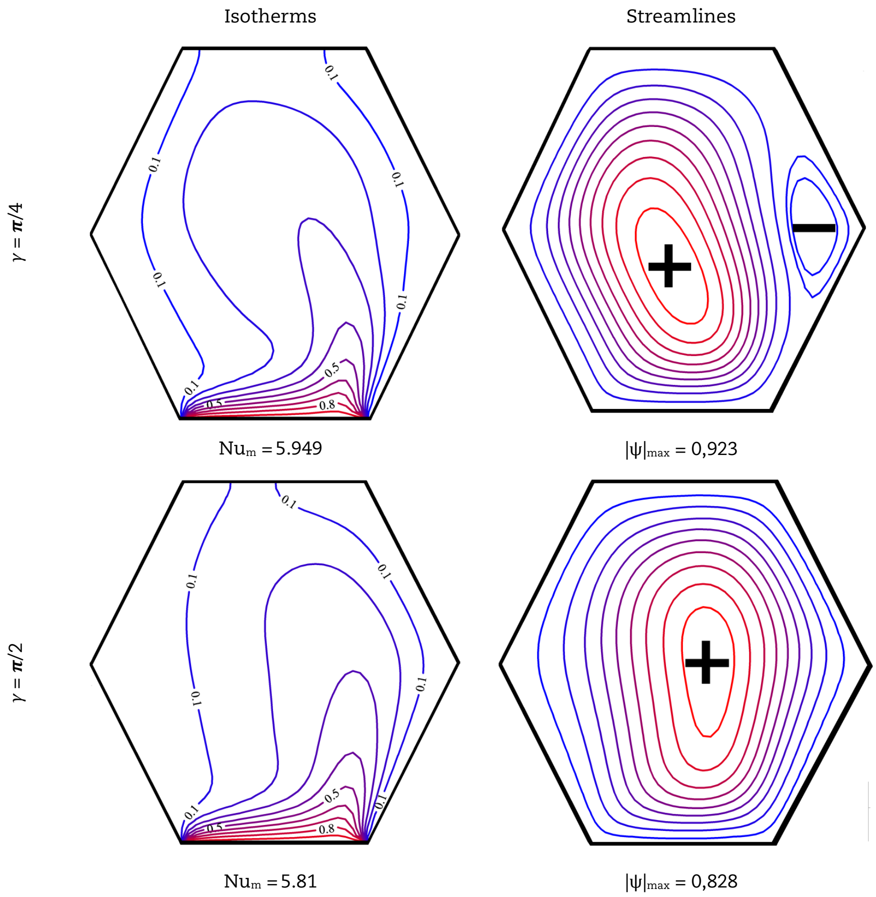

Fig. 15. Isotherms (left) and streamlines (right) for various γ at ϕ = 0,04, Ra = 10^5, and Ha = 0.

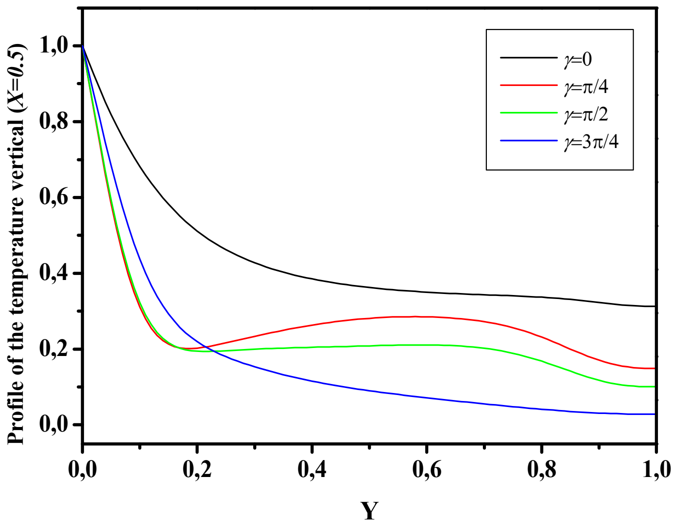

Fig. 16. Profile of the dimensionless temperature in the middle of the cavity (X = 0,5) for different γ at Ra = 10^5, Ha = 0 and ϕ = 0,04.

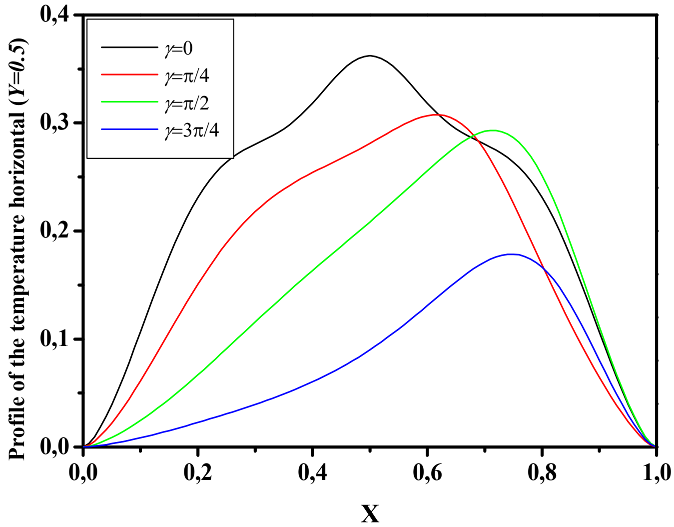

Fig. 17. Profile of the dimensionless temperature in the middle of the cavity (Y = 0,5) for different γ at Ra = 10^5, Ha = 0 and ϕ = 0,04.

This change is particularly noticeable when γ reaches $\pi/4$. At this point, the two initially distinct cells tend to merge into a single dominant cell, redistributing the hot and cold fluid within the cavity. The isotherms then stretch toward the inclined walls (*BC* and *CD*), indicating increased displacement of hot fluid toward the regions adjacent to these walls. This is clearly highlighted by the evolution of the temperature profiles: at the mid-position Y = 0,5 and vertical at the mid-position X = 0,5, for Ra = 10^5 and Ha = 0 (uniform) (Figs. 16 and 17).

This phenomenon reflects a local enhancement of heat transfer by convection in these specific areas. In contrast, along the two opposing walls (*EF* and *FA*), the opposite effect is observed: convection becomes less effective as γ increases, resulting in reduced heat transfer. This evolution highlights the crucial influence of inclination on the thermal dynamics of the system, where local heat transfer conditions can be either enhanced or weakened depending on the relative orientation of the cavity.

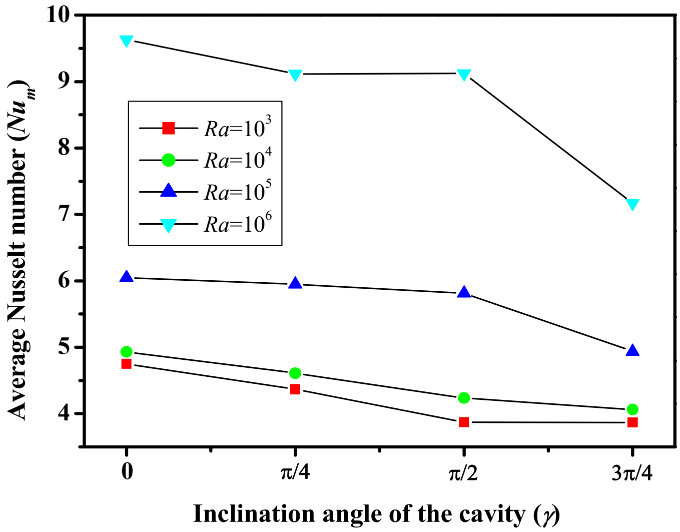

Fig. 18. Average Nusselt number on the hot wall for different γ at $Ra = 10^5$, $Ha = 0$ and $\phi = 0{,}04$.

Figure 18 shows the variation of the average Nusselt number as a function of the inclination angle γ. These results reveal that increasing the inclination angle γ has a notable impact on heat transfer, leading to a gradual reduction in the heat transfer rate. This behavior can be explained by the alteration of convection mechanisms within the cavity, which becomes less efficient as the inclination angle increases. This decrease in the heat transfer rate is particularly significant for $Ra = 10^6$.

7. Conclusion

This study presented an innovative approach to examining convective heat transfer by analyzing the impact of a periodic magnetic field on the heat transfer and flow characteristics in a hexagonal cavity filled with an Al_2O_3-Ag-water nanohybrid. The effects of the Rayleigh number (Ra), Hartmann number (Ha), magnetic field period (λ), cavity tilt angle (γ), and nanoparticle volume fraction (ϕ) on flow and heat transfer characteristics were investigated. The main conclusions drawn from the numerical results are as follows:

- For all considered values of Ra, Ha, λ, and γ, increasing the nanoparticle volume fraction leads to an increase in the average Nusselt number.
- The average Nusselt number increases with the Rayleigh number (Ra), while the Hartmann number and cavity tilt angle have opposite effects.
- The application of a uniform magnetic field reduces the heat transfer by 42,77% for $Ha = 40$.
- A higher average heat transfer rate is observed under the effect of a non-uniform vertical magnetic field when $\lambda = 0{,}75$, with an increase of 14,52% compared to the case with a uniform vertical magnetic field for $Ha = 40$.
- When horizontal magnetic field is applied for $Ha = 40$, an optimal average heat transfer rate can be achieved at $\lambda = 0{,}5$, which results in the lowest heat transfer rate.
- The effect of the tilt angle γ on heat transfer is more significant at high Rayleigh numbers ($Ra = 10^6$), leading to a decrease in heat transfer of more than 31% when γ changes from zero to $3\pi/4$.

Author Contributions

B. Mliki mathematically formulated the problem in order to design a framework for the internal source code. M. Ferhi developed the FORTRAN code, conducted the simulation tests, and validated the code's accuracy. Subsequently, simulations were performed to extract the data presented in the paper. The first version of the manuscript was written by M.A. Abbassi, and after discussing the results, the authors collaborated to finalize the manuscript. The manuscript was written through the contribution of all authors. All authors discussed the results, reviewed, and approved the final version of the manuscript.

Acknowledgments

Not Applicable.

Conflict of Interest

The authors declared no potential conflicts of interest concerning the research, authorship, and publication of this article.

Funding

The authors received no financial support for the research, authorship, and publication of this article.

Data Availability Statements

The datasets generated and/or analyzed during the current study are available from the corresponding author on reasonable request.

Nomenclature

B	Magnetic field [N/(A.m^2)]
c	Lattice speed [m/s]
c_s	Speed of sound [m/s]
c_i	Discrete particle speed [m/s]
C_p	Specific heat at constant pressure [J.kg^{-1}.K^{-1}]
f_i^{eq}	Equilibrium distribution function for flow field
F_i	External forces [N]
g	Gravitational acceleration [m/s^2]
g_i^{eq}	Equilibrium distribution function for temperature
Ha	Hartmann number
k	Thermal conductivity [W.m^{-1}K^{-1}]
L	Length of the cavity [m]
H	characteristic length[m]
p	Fluid pressure [N/m^2]
Nu_m	Average Nusselt number
Nu	Local Nusselt number
P	Pressure [Pa]
Pr	Prandtl number
Ra	Rayleigh number
Ri	Richardson number
T	Temperature [K]
u,v	Velocity components [m.s^{-1}]
x,y	Lattice coordinates [m]

Greek letters

α	Thermal diffusivity [m^2.s^{-1}]
β	Thermal expansion coefficient [K^{-1}]
γ	Inclination angle of the cavity
θ	Non-dimensional temperature
λ	Magnetic field period
λ_h	Magnetic horizontal field period
λ_v	Magnetic vertical field period
μ	Dynamic viscosity [kg.m^{-1}.s^{-1}]
ρ	Fluid density [kg.m^{-3}]
σ	Electrical conductivity [Ω.m^{-1}]
τ_ν	Lattice relaxation time for flow field [s]
τ_α	Lattice relaxation time for temperature [s]
ϕ	Solid volume fraction
ψ	Stream function [m^2.s^{-1}]

Subscripts

T_h	Hot temperature
T_c	Cold temperature
n_h	Hybrid-nanofluid

Abbreviations

MHD	Magnetohydrodynamics
LBM	Lattice Boltzmann Method
CFD	Computational Fluid Dynamics

References

[1] Hollands, K.G.T., Honeycomb devices in flat-plate solar collectors, *Solar Energy*, 9(3), 1965, 159–164.
[2] Buchberg, H., Edwards, D.K., Mackenzie, J.D., *Transparent Glass Honeycombs for Energy Loss Control*, School of Engineering and Applied Science, University of California, Los Angeles, CA, USA, 1977.
[3] Sheikholeslami, M., Said, Z., Jafaryar, M., Hydrothermal analysis for a parabolic solar unit with wavy absorber pipe and nanofluid, *Renewable Energy*, 188, 2022, 922–932.
[4] Islam, S., Bairagi, T., Islam, T., Rana, B.M.J., Reza-E-Rabbi, S.K., Rahman, M.M., Heatline visualization in hydromagnetic natural convection flow inside a prismatic heat exchanger using nanofluid, *International Journal of Thermofluids*, 16, 2022, 100248.
[5] Nilankush, A., Ali, J.C., On the magnetohydrodynamic Al2O3-water nanofluid flow through parallel fins enclosed inside a partially heated hexagonal cavity, *International Communications in Heat and Mass Transfer*, 132, 2022, 105885.
[6] Hussain, F., Othman, M.Y.H., Yatim, B., A study of PV/T collector with honeycomb heat exchanger, *AIP Conference Proceedings*, 10, 2013, 1571.
[7] Mozumder, A., Singh, A.K., Sharma, P., Study of cylindrical honeycomb solar collector, *Journal of Solar Energy*, 10, 2014, 539894.
[8] Majeed, A.H., Mahmood, R., Shahzad, H., Pasha, A., Islam, N., Rahman, M.M., Numerical simulation of thermal flows and entropy generation of magnetized hybrid nanomaterials filled in a hexagonal cavity, *Case Studies in Thermal Engineering*, 39, 2022, 102293.
[9] Nayak, M.K., Dogonchi, A.S., Rahbari, A., Free convection of Al2O3-water nanofluid inside a hexagonal-shaped enclosure with cold diamond-shaped obstacles and periodic magnetic field, *Case Studies in Thermal Engineering*, 50, 2023, 103429.
[10] Alam, M.S., Huda, M.N., Rahman, M.M., Billah, M.M., Statistical and numerical analysis of magnetic field effects on laminar natural convection heat transfer of nanofluid in a hexagonal cavity, *International Journal of Thermofluids*, 24, 2024, 100856.
[11] Saleh, M.A., Thermal investigation of nanofluid-filled hexagonal fillet cavity under the influence of heated and concentric cylinder, *Case Studies in Thermal Engineering*, 49, 2023, 103180.
[12] Khan, Y., Majeed, A.H., Shahzad, H., Awan, F.J., Iqbal, K., Ajmal, M., Faraz, N., Numerical computations of non-Newtonian fluid flow in hexagonal cavity with a square obstacle: a hybrid mesh–based study, *Frontiers in Physics*, 10, 2022, 891163.
[13] Gowtham, S., Sivaraj, C., Sheremet, M.A., Analysis of magneto-natural convection and second law of thermodynamics of Cu-Al2O3-hybrid nanofluid in a vertical wavy cabinet having a localized non-uniform heat source, *Journal of Magnetism and Magnetic Materials*, 610, 2024, 172416.
[14] Muhammad, S.K., Shafee, A., Zahir, S., Vrinceanu, N., Mansoor, H., Natural convection heat transfer of a hybrid nanofluid in a permeable quadrantal enclosure with heat generation, *Case Studies in Thermal Engineering*, 56, 2024, 104207.
[15] Islam, Md. S., Islam, S., Noor-A-Alam, S., Numerical simulation with sensitivity analysis of MHD natural convection using Cu-TiO2-H2O hybrid nanofluids, *International Journal of Thermofluids*, 20, 2023, 100509.
[16] Arifin, N.Md., Saleh, H., Azizul, F.M., Casson hybrid nanofluid natural convection in trapezoidal cavity containing a partially heated wall, *Journal of Advanced Research in Fluid Mechanics and Thermal Sciences*, 100(2), 2022, 78–95.
[17] Mliki, B., Abbassi, M.A., Entropy generation of MHD natural convection heat transfer in a heated incinerator using hybrid-nanoliquid, *Propulsion and Power Research*, 10, 2021, 143–154.
[18] Khan, N.H., Paswan, M.K., Hassan, M.A., Natural convection of hybrid nanofluid heat transport and entropy generation in cavity by using Lattice Boltzmann Method, *Journal of the Indian Chemical Society*, 99(3), 2022, 100344.
[19] Bouchmel, M., Mohamed, A.A., Fateh, M.O., Simulation of magnetic hybrid nanofluid (Al2O3-Cu/H2O) effect on natural convection and entropy generation in a square enclosure with a hot obstacle, in *Mathematical Modelling of Fluid Dynamics and Nanofluids*, CRC Press (Taylor & Francis), 2023.
[20] Haque, M.M., Alam, M.S., Natural convective heat transfer of Al2O3-Cu/water hybrid nanofluid in a rectotrapezoidal enclosure under the influence of periodic magnetic field, *International Journal of Thermofluids*, 22, 2024, 100661.
[21] Mliki, B., Abbassi, M.A., Omri, A., Zeghmati, B., Augmentation of natural convective heat transfer in linearly heated cavity by utilizing nanofluids in the presence of magnetic field and uniform heat generation/absorption, *Powder Technology*, 284, 2015, 312–325.
[22] Miri, R., Mliki, B., Mohamad, B.A., Abbassi, M.A., Oreijah, M., Guedri, K., Abderafi, S., Entropy generation and heat transfer rate for MHD forced convection of nanoliquid in presence of viscous dissipation term, *CFD Letters*, 15(12), 2023, 77–106.

[23] Miri, R., Abbassi, M.A., Ferhi, M., Djebali, R., Second law analysis of MHD forced convective nanoliquid flow through a two-dimensional channel, *Acta Mechanica et Automatica*, 4, 2022, 417–431.
[24] Das, P., Hasan Mamun, M.A., Predicting MHD mixed convection in a semicircular cavity with hybrid nanofluids using AI, *Heliyon*, 10, 2024, 38303.
[25] Abood, F.A., Radhi, Z.K., Hadi, A.K., Homod, R.Z., Mohammed, H.I., MHD mixed convection of nanofluid flow Ag-Mgo/water in a channel containing a rotational cylinder, *International Journal of Thermofluids*, 22, 2024, 100713.
[26] Mliki, B., Abbassi, M.A., Analysis of natural convection under the effect of nanoparticles Brownian motion and a periodic magnetic field utilizing CuO–water nanofluid, *Journal of Nanofluids*, 13, 2024, 1123–1133.
[27] Omle, I., Kovács, E., Betti, B., The effect of surface triangular roughness inspired by nature with different angles on the interaction between free convection and surface radiation in a square cavity, *Heat Transfer Research*, 55(5), 2023, 1–21.
[28] Ighris, Y., Qaffou, M., Baliti, J., Elguennouni, Y., Hssikou, M., Thermal management optimization of natural convection in a triangular chamber: role of heating positions and ternary hybrid nanofluid, *Physics of Fluids*, 36, 2024, 092002.
[29] Ighris, Y., Bouhouchi, Y., Baliti, J., Hssikou, M., Boumezzough, A., Numerical study of natural convection in an inclined cavity filled with Al2O3/Cu-H2O nanofluids, *Numerical Heat Transfer, Part A: Applications*, 2024, https://doi.org/10.1080/10407782.2024.2314230.
[30] El Hadoui, B., Kaddiri, M., Double Diffusive Natural Convection with Variable Properties of Nanofluid Using Lattice Boltzmann Method, *In: Ali-Toudert, F., Draoui, A., Halouani, K., Hasnaoui, M., Jemni, A., Tadrist, L. (eds) Advances in Thermal Science and Energy, JITH 2022, Lecture Notes in Mechanical Engineering*, Springer, 2024.
[31] Mliki, B., Abbassi, M.A., Omri, A., Lattice Boltzmann simulation of magnetohydrodynamics natural convection in an L-shaped enclosure, *International Journal of Heat and Technology*, 34(4), 2016, 565–573.
[32] Hanif, H., Liang, R., Mahat, R., Dynamics of Ag–TiO2/water hybrid nanofluid flow over a Riga plate, *Case Studies in Thermal Engineering*, 64, 2024, 105348.
[33] Aljabali, A., Kasim, A.R.M., Khashi'ie, N.S., Waini, I., Ariffin, N.A.N., Stagnation flow of Eyring-Powell hybrid Cu-Al2O3/water nanofluid towards a Riga plate with Newtonian heating, *Journal of Applied and Computational Mechanics*, 11(1), 2025, 110–119.
[34] Mliki, B., Miri, R., Djebali, R., Abbassi, M.A., CuO–water MHD mixed convection analysis and entropy generation minimization in double-lid–driven U-shaped enclosure with discrete heating, *Acta Mechanica et Automatica*, 17(1), 2023, 112–123.
[35] Thilagavathi, A., Prasad, V.R., Thermal heat transfer enhancement analysis of magnetic ternary hybrid nanofluid in a hexagonal cavity with square obstacle, *Journal of Applied and Computational Mechanics*, 11(1), 2025, 239–252.
[36] Ferhi, M., Djebali, R., Al Kouz, W., Abboudi, S., Chamkha, A.J., MHD conjugate heat transfer and entropy generation analysis of MWCNT/water nanofluid in a partially heated divided medium, *Heat Transfer*, 50(1), 2021, 126–144.
[37] Mejri, I., Mahmoudi, A., Abbassi, M.A., Omri, A., LBM simulation of natural convection in an inclined triangular cavity filled with water, *Alexandria Engineering Journal*, 55, 2016, 1385–1394.
[38] Jannat Asha, N.E., Molla, Md. M., MRT-lattice Boltzmann simulation of MHD natural convection of Bingham nanofluid in a C-shaped enclosure with response surface analysis, *Heliyon*, 9, 2023, 22539.
[39] Ghasemi, B., Aminossadati, S.M., Raisi, A., Magnetic field effect on natural convection in a nanofluid-filled square enclosure, *International Journal of Thermal Sciences*, 50, 2011, 1748–1756.

ORCID iD

Bouchmel Mliki https://orcid.org/0000-0002-0200-8060
Mokhtar Ferhi https://orcid.org/0000-0002-6677-3335
Mohamed A. Abbassi https://orcid.org/0000-0002-1915-0944

How to cite this article: Mliki B., Ferhi M., Abbassi M.A. Effect of a Periodic Magnetic Field on Natural Convection in a Hexagonal Cavity Containing a Nanohybrid Fluid, *J. Appl. Comput. Mech.*, 12(1), 2026, 255-270. https://doi.org/10.22055/jacm.2025.48166.5025